Annu. Rev. Phys. Chem. 2005. 56:1–23
doi: 10.1146/annurev.physchem.56.092503.141319

First published online as a Review in Advance on September 27, 2004

QUANTUM CHAOS MEETS COHERENT CONTROL

Jiangbin Gong[1] and Paul Brumer[2]
[1]*Department of Chemistry and The James Franck Institute, The University of Chicago, Chicago, Illinois 60637; email: jbgong@uchicago.edu*
[2]*Chemical Physics Theory Group, Department of Chemistry, and Center for Quantum Information and Quantum Control, University of Toronto, Toronto, Canada M5S 3H6; email: pbrumer@tikva.chem.utoronto.ca*

Key Words quantum-classical correspondence, delta-kicked dynamics, anomalous diffusion, ratchet accelerator, photodissociation

■ **Abstract** Coherent control of atomic and molecular processes has been a rapidly developing field. Applications of coherent control to large and complex molecular systems are expected to encounter the effects of chaos in the underlying classical dynamics, i.e., quantum chaos. Hence, recent work has focused on examining control in model chaotic systems. This work is reviewed, with an emphasis on a variety of new quantum phenomena that are of interest to both areas of quantum chaos and coherent control.

1. INTRODUCTION

Over the past two decades there have been great advances in the active control of atomic and molecular processes by use of the quantum nature of the light-matter interaction (1–6). The key idea that motivated this exciting field, now widely known as "coherent control," is that quantum coherence effects that are absent in classical molecular dynamics can be manipulated via experimentally controllable parameters to control the dynamics. For example, laser phases can be imprinted on the relative quantum mechanical phase between different excitation pathways to the same target state (7), or coherently encoded in laser pulses (8), resulting in experimentally controllable quantum interference effects that can be useful, dramatic, and even counter-intuitive. Coherent control methods also provide an interesting approach to revealing and understanding new aspects of the quantum nature of molecular dynamics (9–11). To date, coherent control has been most successfully applied to unimolecular processes such as photodissociation reactions, although the theory and computational applications to bimolecular processes are now mature subjects (1).

Classical unimolecular reaction rate theory teaches us that the classical dynamics associated with unimolecular reactions is nonintegrable in general (12–15). As the reaction energy increases, chaotic behavior, i.e., the exponential sensitivity

of phase space trajectories to slight changes of the initial conditions (16, 17), arises with few exceptions. In such cases the classical molecular dynamics displays stochasticity that is induced by the dynamics itself and therefore allows for statistical descriptions of the reaction rate. Indeed, the key assumption in a variety of classical statistical treatments of unimolecular reaction rate is precisely the exponential loss of the memory of initial conditions (14, 15, 18).

Thus, coherent control studies and classical unimolecular reaction studies are in sharp contrast: the former stress quantum effects and nonstatistical behavior that can be controlled by external control fields, whereas the latter treat the dynamics classically and emphasize the nature of equilibrium statistics in the absence of external fields. This naturally brings up the important question as to whether one can apply coherent control to classically chaotic molecular systems (19). This involves: (*a*) the formal issue of controllability in quantum mechanical systems (20–22), (*b*) practical issues of control in quantum systems, and (*c*) consideration of the general features of the quantum dynamics in classically chaotic systems, the main subject of the field of "quantum chaos" (23–25).

Quantum-classical correspondence in classically chaotic systems remains an interesting fundamental issue in quantum theory (26–28). Well-established, however, is the fact that quantum systems with a discrete spectrum do not display chaotic behavior in the strict sense (28, 29). That is, even when the underlying classical dynamics is chaotic, the time evolution of a quantum system with a discrete spectrum is necessarily periodic or quasiperiodic. Nonetheless, exponential divergence of adjacent localized wavepackets and local positive Lyapunov exponents do characterize the quantum dynamics of these systems over operational timescales (30, 31). Hence, although quantum control of such systems may be less demanding than classical control in the associated classically chaotic system (19), careful studies are required to gain both quantitative and qualitative insight.

Note that there are two different types of coherent control as applied to dynamical systems: one does not affect the qualitative nature of the underlying classical dynamics, whereas the other uses control fields to change the classical phase space structures, e.g., change the classical dynamics from chaotic to regular. Although the latter can be closely related to controlling classical chaos (32–37), this review is primarily concerned with useful quantum coherence effects that are responsible for the coherent control of quantum chaos.

Coherent control is currently being applied to larger and larger systems to achieve the control of the branching ratio between different chemical products (38), of intramolecular energy transfer (39, 40), and of proton transfer and dynamics in large molecules (41, 42). Because the classical dynamics of the rovibrational motion of large molecules is usually complicated and often at least weakly chaotic, it becomes relevant to examine and understand the nature and feasibility of coherent control in systems that are classically chaotic. This has motivated a number of recent studies, reviewed below, on coherent control in simple model systems whose underlying classical dynamics can be chaotic (43–49). These model systems are still far from realistic representations of molecules, but they embody the essence

of quantum control in chaotic systems and offer new insights into a number of fundamental problems that are of interest to both coherent control and quantum chaos.

Finally it is of some historical interest that coherent control emerged (7, 8) from two research groups engaged in studies of chaotic dynamics. It was precisely the realization that quantum dynamics with a discrete spectrum does not permit chaos that motivated the examination of quantum control. However, it is only recently that quantum control of classically chaotic systems has been addressed, as described below.

2. COHERENT CONTROL IN DELTA-KICKED SYSTEMS

The one-dimensional kicked rotor (KR) model provides a simple example of a system (i.e., a planetary rotor) subject to a control field. It is useful for examining the possibility of coherent control in classically chaotic systems for the following reasons. First, the KR and its classical limit, the standard map, have long served as paradigms for quantum and classical chaos (23). Both the classical and quantum dynamics of the KR, which can be readily solved numerically, are extremely rich. Second, there are ongoing experiments on the KR using atom optics techniques (50–53). Third, the KR may be also realized by diatomics in microwave fields or laser fields and should be of great interest to the study of molecular orientation and alignment dynamics (54–56).

Consider the KR Hamiltonian

$$H^{KR}(\hat{L}, \theta, t) = \hat{L}^2/2I + \lambda \cos(\theta) \sum_n \delta(t/T - n), \qquad 1.$$

where $\hat{L}$ is the angular momentum operator, θ is the conjugate angle, I is the moment of inertia, λ is the strength of the kicking field, and T is the time interval between kicks. The basis states of the Hilbert space are given by $|m\rangle$, with $\hat{L}|m\rangle = m\hbar|m\rangle$. The quantum KR map operator for propagating from time $(N - 0^+)T$ to time $(N + 1 - 0^+)T$ is given by

$$\hat{F}_{KR} = \exp\left[i\frac{\tau}{2}\frac{\partial^2}{\partial\theta^2}\right]\exp[-ik\cos(\theta)], \qquad 2.$$

with dimensionless parameters $k = \lambda T/\hbar$ and effective Planck constant $\tau = \hbar T/I$. For later use we also define the dimensionless scaled rotational energy as $\tilde{E}_q \equiv \langle\hat{L}^2\rangle\tau^2/2\hbar^2$, where $\langle\cdot\rangle$ represents the average over the quantum ensemble. The classical dynamics of the KR is given by the standard map, which depends only on one parameter $\kappa \equiv k\tau$:

$$\tilde{L}_N = \tilde{L}_{N-1} + \kappa \sin(\theta_{N-1});$$
$$\theta_N = \theta_{N-1} + \tilde{L}_N, \qquad 3.$$

where $\tilde{L} \equiv L\tau/\hbar$ is the scaled c-number angular momentum and $(\tilde{L}_N, \theta_N)$ represents the phase space location of a classical trajectory at $(N + 1 - 0^+)T$. The classical limit of $\tilde{E}_q$ is given by $\tilde{E}_c$, the classical ensemble average of $\tilde{L}^2/2$. An essential difference between quantum and classical maps is that the former has two characteristic parameters τ and k, whereas the latter depends only on their product. As we decrease the magnitude of τ and fix the value of κ, the quantum dynamics approaches the classical limit.

One molecular realization of the KR, proposed almost two decades ago (57, 58), uses periodically kicking microwave fields. In particular, if the characteristic vibrational excitation energy is much higher than the rotational energy level spacing, then the vibrational motion can be regarded as frozen and the Hamiltonian for the rotational motion subject to periodic microwave pulses resembles that of the KR:

$$\hat{H} = \frac{\hat{J}^2}{2I} + \lambda \cos(\theta) \sum_n \Delta\left(\frac{t}{T} - n\right), \qquad 4.$$

where $\hat{J}$ is the angular momentum operator, $\lambda = \mu E_0$ with μ being the molecular electric dipole moment and E_0 being the amplitude of the driving field whose polarization direction defines the z direction, θ is the polar angle, I is the moment of inertia of the molecule about an axis perpendicular to the symmetry axis, and $\Delta(t/T - n)$ is a pulse shape function simulating the delta kicking in the KR. Because the projection of angular momentum onto the z-axis is a constant (set to be zero below), the diatomic rotation motion has only one degree of freedom. Microwave pulses may be realized by an array of phase-locked microwave generators. For sample calculations discussed below, Δ is assumed to take the form

$$\Delta\left(\frac{t}{T} - n\right) = 1 + 2 \sum_{m=1}^{m=m_N} \cos\left[2m\pi\left(\frac{t}{T} - n - 1/2\right)\right], \qquad 5.$$

with $m_N = 7$. Clearly, in the limit of $m_N \to \infty$, one recovers the delta kicks. However, even in this limiting case there are still some interesting differences between a microwave kicked diatomic system and the KR in Equation 1. For example, the polar angle θ ranges from 0 to π, whereas in the planetary rotor $\theta \in [0, 2\pi]$. Hence, both are discussed below.

Another realization of the KR is that it makes use of the induced dipole moment of diatomics subject to an off-resonance strong laser field. Consider a linear molecule interacting with a linearly polarized laser pulse. If the laser field is nonresonant with any vibronic transition, the laser-molecule interaction can be described by an effective Hamiltonian (59):

$$\hat{H} = \frac{\hat{J}^2}{2I} - \frac{E_0^2}{4}(\alpha_\parallel - \alpha_\perp)\cos^2(\theta) g(t), \qquad 6.$$

where $g(t)$ is the envelope function describing a train of Gaussian pulses, and $\alpha_\parallel$ and $\alpha_\perp$ are the components of the polarizability, parallel and perpendicular to

the molecular axis. In the limit of zero pulse width, the Gaussian pulses can be regarded as delta pulses, and a delta-kicked rotor model is realized with a kicking potential $\cos^2(\theta)$.

2.1. Initial State Coherence Effects

Figure 1 displays the Poincaré surfaces of section (16, 17) associated with the classical dynamics of a microwave kicked diatomic system (see Equation 4). It is clear from Figure 1 that when $k\tau \geq 5.0$, the classical dynamics is predominantly chaotic in the entire region of $\tilde{J} \equiv \dot{\theta}T$. This underlying classical chaos seems to suggest that quantum phases that would be embedded in initial states should play a minor role here due to the loss of memory of the initial state. However, this intuition can be totally misleading because it is a classical argument that does not apply to the quantum regime. In fact, although the standard map typically shows unlimited

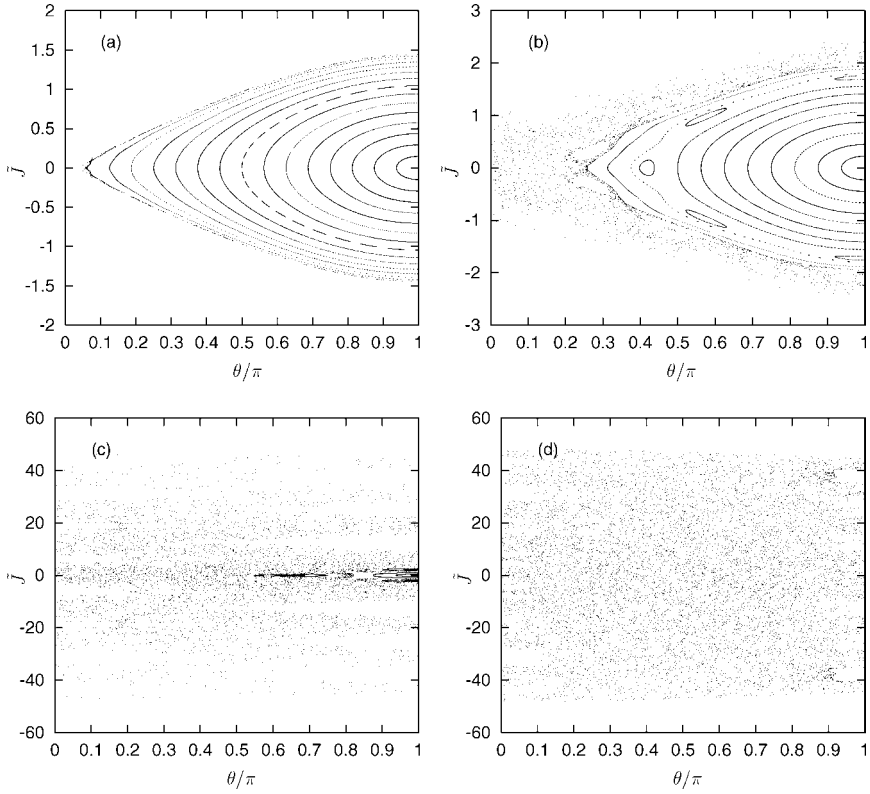

Figure 1 Poincaré surfaces of section for the classical dynamics of a kicked diatomic molecule. (*a*) $k\tau = 0.5$. (*b*) $k\tau = 1.0$. (*c*) $k\tau = 2.5$. (*d*) $k\tau = 5.0$. The classical dynamics is predominantly chaotic when $k\tau \geq 5.0$. From Reference (44) with permission.

linear energy increase due to the underlying classical chaos, the quantum dynamics displays significant suppression of the classical chaotic diffusion. For example, in the quantum KR the external field can only excite a finite number of unperturbed energy levels (23). This phenomenon is called dynamical localization, probably the best known and most studied aspect of quantum chaos in time-dependent systems. This quantum feature of a classically chaotic KR suggests that quantum coherence in the quantum dynamics is important and therefore that various coherent control techniques should be applicable to alter the quantum diffusion in energy space. Gong & Brumer (43, 44) have indeed shown that quantum relaxation dynamics in the KR can be sensitive to the coherence characteristics of the initial state, and that altering these characteristics allows for control over the energy diffusion. The extent of the controlled behavior can be vast, from strong suppression to strong enhancement of diffusion. The same situation exists for the microwave realization of the KR, as discussed below.

Consider an initial superposition state prepared as

$$|\psi(0)\rangle = \cos(\alpha)|j_1, 0\rangle + \sin(\alpha)\exp(-i\beta)|j_2, 0\rangle, \qquad 7.$$

where $|j, 0\rangle$ denotes the angular momentum basis states with zero projection on the z-axis. Of course, more basis states can be considered, providing more adjustable parameters for control. The energy diffusion behavior can be described by the dimensionless rotational energy $\tilde{E} \equiv \sum_j P_j j(j+1)\tau^2/2$, where P_j is the occupation probability of the $|j, 0\rangle$ state.

Figure 2 shows two representative examples ($\tau = 1.0, k = 5.0$ in Figure 2*a*; and $\tau = 1.2$, $k = 4.8$ in Figure 2*b*) of controlled quantum chaotic diffusion in kicked diatomic molecules. The initial superposition state is given by either $(|1, 0\rangle + |2, 0\rangle)/\sqrt{2}$ or $(|1, 0\rangle - |2, 0\rangle)/\sqrt{2}$, with their only difference being the relative phase between the two participating basis states. For both examples,

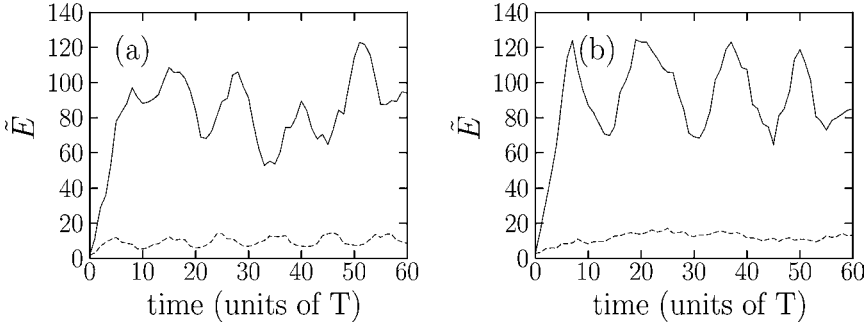

Figure 2 Dimensionless rotational energy of the kicked diatomic molecule $\tilde{E} = \sum_j P_j j(j+1)\tau^2/2$ versus time (in units of T). *Solid line* and *dashed lines* are for the initial states $(|1, 0\rangle + |2, 0\rangle)/\sqrt{2}$ and $(|1, 0\rangle - |2, 0\rangle)/\sqrt{2}$, respectively. (*a*) $\tau = 1.0$, $k = 5.0$. (*b*) $\tau = 1.2$, $k = 4.8$. From Reference (44) with permission.

$(|1,0\rangle - |2,0\rangle)/\sqrt{2}$ results in almost no diffusion over the energy space, whereas $(|1,0\rangle + |2,0\rangle)/\sqrt{2}$ shows extraordinarily fast diffusion [even faster than the semiclassical diffusion with the effective Planck constant significantly decreased (44)] before it essentially stops at $t \approx 10\ T$. Note (*a*) that this huge difference is achieved solely by changing the initial relative phase between the two participating states $|1,0\rangle$ and $|2,0\rangle$ in the initial superposition state, and (*b*) that by contrast, each of $|1,0\rangle$ or $|2,0\rangle$ individually would give very similar diffusion behavior lying between the solid and dashed lines in Figure 2. In effect, states $|1,0\rangle$ and $|2,0\rangle$ can either constructively or destructively interfere with each other, even though the underlying classical dynamics is strongly chaotic. These results are similar to those in the KR (43). Note also that $\beta = 0$ or π always gives the best control due to the time-reversal symmetry of the system (44).

One of the main results of the study of quantum chaos is that statistical properties of eigenfunctions and eigenvalues of the quantum map operator (or of the Hamiltonian operator for conservative systems) tend to be well described by the random matrix theory (RMT) if the underlying classical dynamics is chaotic (24, 25). Indeed, statistical behavior close to RMT predictions is regarded as a clear signature of classical chaos. However, it turns out that RMT does not apply here, as it would suggest that the quantum interference between states $|1,0\rangle$ and $|2,0\rangle$ would be insignificant (44). As such, the above observed control can be interpreted as a strong manifestation of the deviation from RMT.

2.2. Control of Dynamical Localization by Periodic Field Reversal

Control of quantum molecular dynamics can either keep the system Hamiltonian intact or strongly affect the phase space structures associated with the underlying classical dynamics. Control based on initial state coherence effects clearly belongs to the first type. Consider now a simple control scenario of the second type (47), where the kicking field is periodically reversed after a certain number of kicks. Specifically, consider a slightly modified kicked rotor (MKR) system whose Hamiltonian is given by:

$$H^{MKR}(\hat{L},\theta,t) = \hat{L}^2/2I + \lambda\cos(\theta)\sum_n f_M(n)\delta(t/T - n), \qquad 8.$$

where $f_M(n)$ is real, $|f_M(n)| = 1$, and $f_M(n)$ changes sign after every M kicks. That is, the only difference between the KR and MKR is that in the MKR the kicking potential is reversed after every M kicks. The effect of reversing the kicking potential can be seen more clearly by examining the time-evolving wave function, which can be expanded as a superposition of $|m\rangle$ states: $\sum_m C_m\langle\theta|m\rangle$, with expansion coefficients C_m. Because $\cos(\theta+\pi) = -\cos(\theta)$, and $\sum C_m\langle\theta+\pi|m\rangle = \sum_m(-1)^m C_m\langle\theta|m\rangle$, reversing the kicking potential is equivalent to adding a π phase difference between all neighboring basis states. So the field-reversal scenario here is an extension of the previous approach: it introduces quantum phases

into the system periodically. Note that the field reversal can also be effectively realized by introducing a time delay after every M kicks (47).

To understand the control mechanism from a classical dynamics perspective, let us first discuss the so-called transporting trajectories in both the KR and MKR. For particular values of κ, the standard map can generate trajectories whose momentum increases (or decreases) linearly with time. These trajectories are called transporting trajectories (60). To see this, consider the initial conditions: $(\tilde{L} = 2\pi l_1, \theta = \pm\pi/2)$ for $\kappa = 2\pi l_2$, where l_1 and l_2 are integers. Clearly, these phase space points are shifted by a constant value $(\pm 2\pi l_2)$ in $\tilde{L}$ after each iteration, resulting in a quadratic increase of rotational energy. These transporting trajectories are rather stable insofar as they may persist for values of κ close to $2\pi l_2$, thus giving rise to transporting regular islands (60), called the accelerator modes in the KR case (61–63). If classical trajectories are launched from the accelerator modes, they simply jump to other similar islands located in adjacent phase space cells. For trajectories initially outside the accelerator modes, the stickiness of the boundary between the accelerator modes and the chaotic sea induces anomalous diffusion over the energy space, i.e., energy increases in a nonlinear fashion, but not quadratically. This is intrinsically different from the case of normal chaotic diffusion in which energy increases linearly with the number of kicks.

Dramatically, for the classical MKR with $M = 2$ (46), there exist novel types of transporting trajectories that are different from those in the KR (46). In particular, for $\kappa = (2l_2 + 1)\pi$, trajectories emanating from $\tilde{L} = (2l_1 + 1)\pi, \theta = \pm\pi/2$ will be shifted by a constant value $[\pm(2l_2 + 1)\pi]$ in $\tilde{L}$ after each kick. This observation suggests that transporting regular islands that differ from the accelerator modes in the KR can be created by reversing the kicking potential after every two kicks. Figure 3 displays the classical phase space structures of both the KR and the MKR with $M = 2$, for $\kappa = 5.0$ (*a* and *b*) and $\kappa = 3.5$ (*c* and *d*). The regular islands seen in Figures 3*a* and 3*c* (the KR case) are not transporting because the momentum of the trajectories launched from these islands is bounded and oscillates periodically. By contrast, a simple computation reveals that the small islands seen in Figures 3*b* and 3*d* in the MKR case are transporting. Classical trajectories launched from the right (left) regular region shown in Figures 3*b* and 3*d* have their momentum shifted by π $(-\pi)$ on the average after each kick, indicating that these regular regions originate from the marginally stable point $\tilde{L} = (2l_1 + 1)\pi, \theta = \pm\pi/2$ with $\kappa = \pi$. Hence, in this case the periodic field reversal in going from the KR to the MKR has both destroyed the nontransporting regular islands of the KR and induced new transporting regular islands. Note that the transporting islands shown in Figure 3*d* are much larger than the well-studied accelerator modes in the KR. Interesting transporting islands are also found in cases where the kicking potential is reversed after every $M > 2$ kicks where $M = 6, 10, 14 \ldots$. However, in these cases the transporting regular islands are much smaller and are extremely sensitive to the value of κ.

Figure 4 displays energy absorption of the MKR with $M = 2$ for the case of $\tau = 1.0$, $k = 5.0$. Here the effective Planck constant is at least one order of

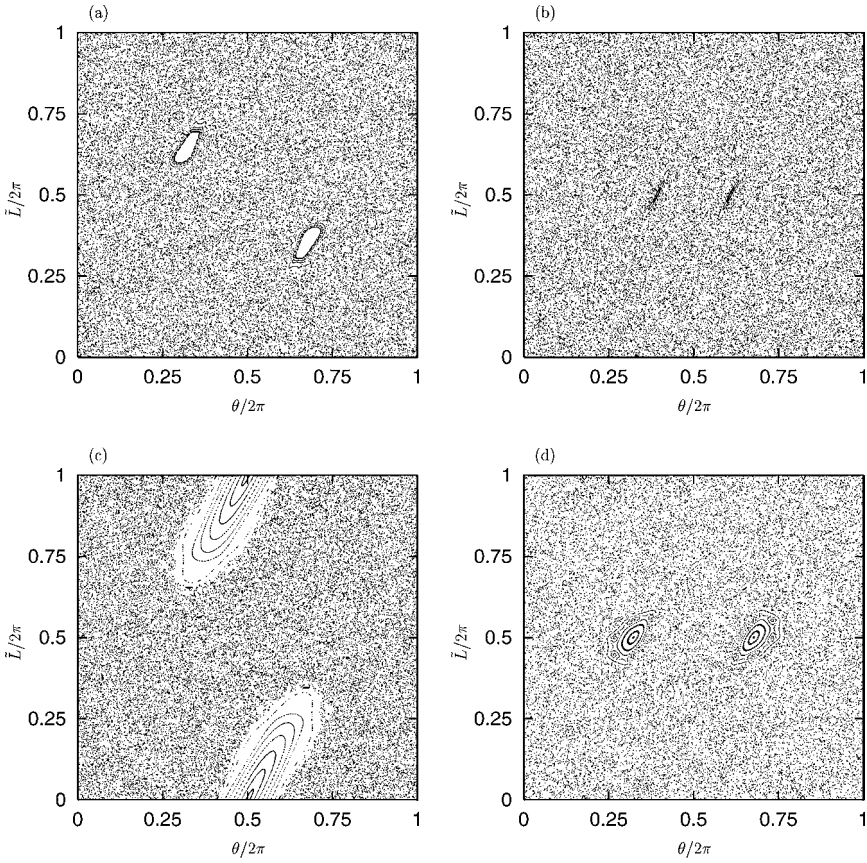

Figure 3 A comparison of classical phase space structures between the standard map and the MKR map with $M = 2$, in the case of $\kappa = 5.0$ (*a* and *b*) and $\kappa = 3.5$ (*c* and *d*). All variables are in dimensionless units. Note that the regular islands seen in *b* and *d* are transporting whereas those in *a* and *c* are not.

magnitude larger than the area of the regular islands in Figure 3*b*. Intuitively, one would anticipate that such transporting regular islands are too small to be relevant to the quantum dynamics. Surprisingly, this intuition is incorrect. As shown in Figure 4, the energy absorption associated with the MKR with $M = 2$ (*upper dashed line*) is much larger than that of the KR (*solid line*). Consider, for example, $\tilde{E}$ at a specific time $t = 1500\,T$ when the energy absorption of both the KR and MKR has clearly shown signs of saturation: $\tilde{E} = 67.7$ for the KR and $\tilde{E} = 1269.7$ for the MKR. Thus, a control factor larger than an order of magnitude has been achieved in going from the KR Hamiltonian to the MKR case with $M = 2$. To confirm that this control is uniquely related to the transporting islands in the classical phase space, Figure 4 also shows the result in the MKR case with $M = 3$,

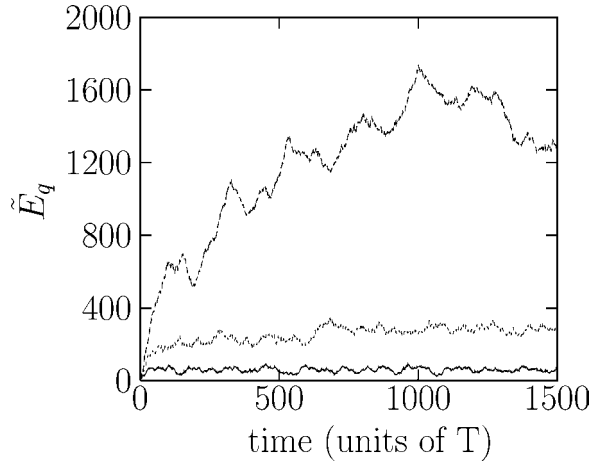

Figure 4 Time dependence of the dimensionless scaled rotational energy $\tilde{E}_q$ for KR (*solid line*), for the MKR with $M = 2$ (*upper dashed line*), and for the MKR with $M = 3$ (*middle dashed line*), with $\tau = 1.0$, $k = 5.0$, and the initial state $|0\rangle$. From Reference (47) with permission.

whose energy absorption is slightly faster than the KR case, but much slower than the $M = 2$ case.

The significant results in Figure 4 suggest that although coherent control relies on quantum coherence effects that are absent in classical dynamics, classical phase space structures may be very useful in understanding and designing simple control scenarios. This can be the case even when the classical dynamics is primarily chaotic and the quantum dynamics is in the deep quantum regime.

The field reversal control scenario also offers new opportunities for studying quantum correlations and fluctuations in quantum chaos. Consider now the characteristic lineshape of the distribution function $P(m)$ versus m long after the energy absorption in the quantum KR or MKR system has saturated, where $P(m)$ is the probability of finding the system in state $|m\rangle$. It is well known that dynamical localization of the KR can be mapped onto the problem of Anderson localization in disordered systems (64) and that an exactly soluble case of disorder in tight-binding models (65) suggests that dynamical localization should assume an exponential lineshape. However, due to some subtle quantum phase correlations in the quantum dynamics, nonexponential dynamical localization lineshapes in the KR are also expected to exist, which were previously observed in the KR for some particular system parameters (61, 66). Interestingly, intriguing differences in the dynamical localization lineshape can be created by simply reversing the kicking potential after every two kicks (47). A sample result is shown in Figure 5, which compares the broad nonexponential dynamical localization lineshapes in the MKR to the analogous narrow exponential lineshapes in the KR, for four different values of k and τ. As shown in Figure 5, in the MKR case, $P(m)$ plotted in the log scale

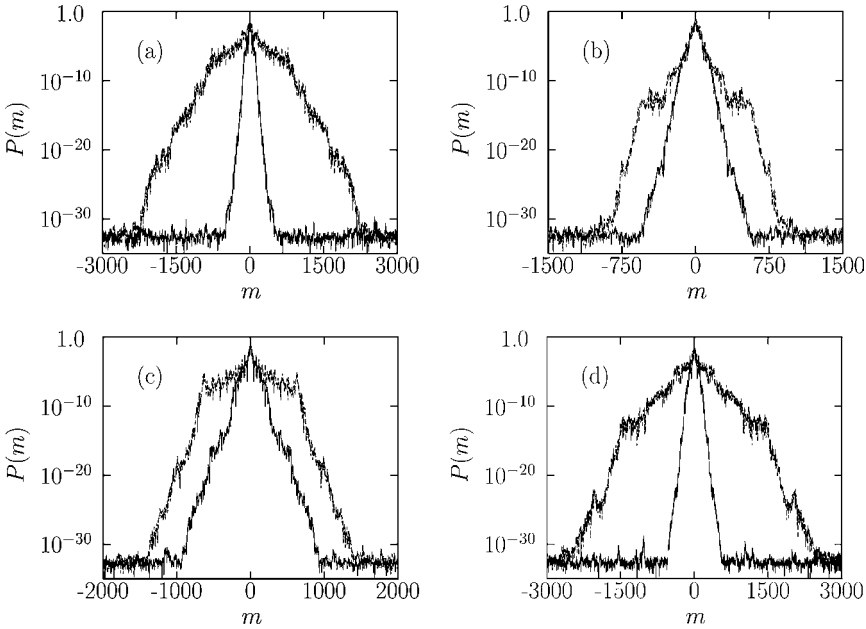

Figure 5 Four examples of nonexponential lineshapes for dynamical localization in the MKR with $M = 2$, shown in terms of the probability $P(m)$ of finding the system in the state $|m\rangle$ after 8000 kicks, with the initial state $|0\rangle$. The results will remain the same for longer times. The MKR results are represented by upper *dashed lines* (the broad lineshape) and, for the purpose of comparison, the corresponding results in the KR case are also shown here and represented by *solid lines* (the narrow lineshape). (*a*) $\tau = 1.0$, $k = 5.0$, (*b*) $\tau = 2.0$, $k = 5.0$, (*c*) $\tau = 1.0$, $k = 5.7$, and (*d*) $\tau = 2.0$, $k = 6.0$. (From Reference 47 with permission.) Note the log scale on the ordinate.

displays structures that are far from purely exponential. For example, one sees that the initial exponential decay rate of $P(m)$ is considerably smaller than that for large $|m|$, suggesting that multiple characteristic lengths are needed to describe dynamical localization in the MKR. Also seen is that the difference in $P(m)$ between the KR and MKR can be as large as ten orders of magnitude or more. We anticipate that results here should motivate an increasing interest in characterizing and understanding nonexponential dynamical localization. Note however, that all the lineshapes shown in Figure 5 are symmetric, i.e., $P(m) = P(-m)$. As seen in Section 2.4 below, this property disappears in the presence of a second symmetry-breaking kicking field.

2.3. Faster-Than-Classical Anomalous Diffusion

Consider now quantum versus classical energy absorption behavior in cases where the effective Planck constant (e.g., $\tau = 0.1$) is smaller than the area of the transporting islands (46). We choose $\kappa = 3.5$ as an example; the associated classical

phase space structures in the KR and MKR with $M = 2$ have been shown in Figures 3*c* and 3*d*. Consider the case where the initial quantum state is chosen to be $|0\rangle$, which evidently does not overlap the transporting islands. The corresponding classical initial state is given by $\tilde{L} = 0$ with θ uniformly distributed over $[0, 2\pi]$. Figure 6*a* displays the quantum-classical comparison in the KR case. Clearly, quantum effects in the KR strongly suppress classical energy absorption and the quantum-classical-correspondence (QCC) break time t_b^{KR} in Figure 6*a* is $\sim 20\,T$. By contrast, Figure 6*b* shows that both the quantum and classical MKR systems display characteristics of anomalous diffusion: an excellent log-log linear fit of the results in Figure 6*b* after the MKR QCC break time (denoted t_b^{MKR}) gives that $\tilde{E}_q \propto N^{1.85}$ (*solid line*) and $\tilde{E}_c \propto N^{1.36}$ (*dashed line*), where N is the number of kicks. Hence, significantly, the quantum energy absorption is seen to be far greater than that associated with the underlying classical anomalous diffusion. This rapid quantum growth is even more visible in Figure 6*c*, which shows that the faster-than-classical excitation process shown in Figure 6*b* persists for much longer timescales, as well as for an effective Planck constant that is 10 times smaller (see the discrete points in Figure 6*c*). Also evident in Figure 6*c* is that a smaller effective Planck constant gives better QCC. Thus, counter-intuitively, the quantum anomalous diffusion here approaches the underlying classical anomalous diffusion from above rather than from below as the effective Planck constant goes to zero. This is quite different from the standard picture of quantum suppression of classical chaotic diffusion.

This faster-than-classical anomalous diffusion may be explained in terms of a quantum tunneling mechanism (46, 62). At early times, both the quantum and classical systems that are not initially on the transporting regular islands tend to stick to the fractal structures lying between the main transporting regular islands and the chaotic sea, resulting in excellent QCC in anomalous diffusion. Later, for $t \sim t_b^{MKR}$, a non-negligible part of the time-evolving quantum state tunnels from the chaotic sea to the large transporting islands, whereas each classical trajectory can at most continue to sojourn in the neighborhood of the transporting islands for a certain time. Thus, if the mean sojourn time of classical trajectories is relatively short compared to the characteristic timescale over which the transporting-island component of the time-evolving quantum state builds up and then tunnels back to the chaotic sea, the quantum tunneling effects can strongly enhance the transport in phase space, and therefore quantum anomalous diffusion can be significantly faster than classical anomalous diffusion. This also makes it clear that quantum anomalous diffusion in the MKR will slow down and dynamical localization can take place when significant tunneling in the reverse direction (i.e., from the transporting islands to the chaotic sea) occurs.

This mechanism of faster-than-classical anomalous diffusion indicates that in controlling classically chaotic quantum dynamics, advantage may be taken of quantum tunneling to make use of certain classical phase space structures, even when these structures are not dynamically reachable in the classical dynamics. Such effects have dramatic consequences in energy absorption behavior. Figure 7

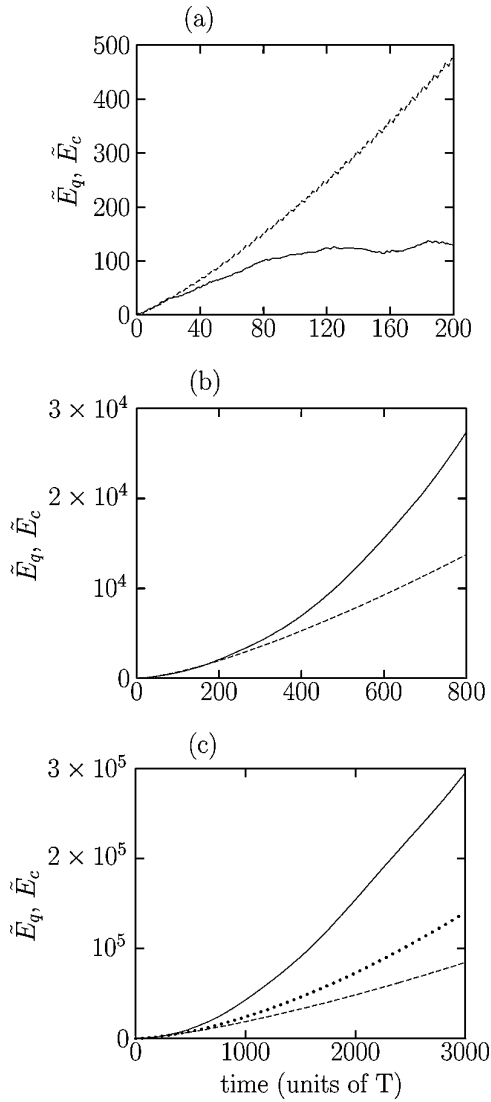

Figure 6 Time dependence of the average dimensionless scaled rotational energy, denoted by $\tilde{E}_q$ and $\tilde{E}_c$ for quantum and classical ensembles, respectively, for (*a*) KR, (*b*) MKR with $M = 2$, and (*c*) MKR over even longer timescales, with $\kappa = 3.5$. *Solid lines* denote quantum results for $\tau = 0.1$, *dashed lines* denote classical results. The discrete points in (*c*) represent quantum results for $\tau = 0.01$. Note that in (*b*) and (*c*) quantum results are well above the classical results. From Reference (46) with permission.

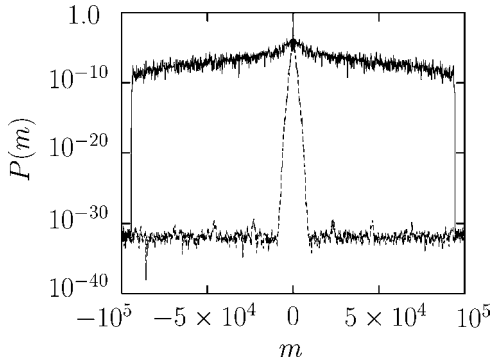

Figure 7 Control of energy absorption behavior by reversing the kicking field after every two kicks. Shown here is a comparison between KR (*dashed line*) and MKR (*solid line*) in terms of the probability $P(m)$ of finding the system in the state $|m\rangle$ at $t = 3000\,T$. $\kappa = 3.5$, $\tau = 0.1$, and the initial state is $|0\rangle$. From Reference (46) with permission.

displays a comparison between the KR and the MKR with $M = 2$ in terms of the occupation probability $P(m)$ of $|m\rangle$ after 3000 kicks, with $\kappa = 3.5$, $\tau = 0.1$, and the initial state $|0\rangle$. It is seen that, for many states (e.g., for $90000 > |m| > 8000$), $P(m)$ of the MKR is 10^{20} larger than that of the KR. It should be stressed that this vast quantum control over energy absorption is achieved by simply reversing the kicking potential, or, alternatively, by introducing a certain time delay after every two kicks, and that the control mechanism here is uniquely based upon quantum anomalous diffusion in the MKR, and is thus far more effective than that in the amplitude-modulated KR (67, 68) or the phase-modulated KR (47) in the absence of transporting islands.

2.4. Ratchet Accelerator

Ratchet effects, i.e., directed transport without external bias due to a broken spatial-temporal symmetry, are of great interest in the understanding of molecular rotors in biological systems and have been under intense investigation using a variety of simple model systems (69, 70). Early studies focused on the role of external noise, which was then replaced by deterministic chaotic dynamics with dissipation (71–74). Recently, it was shown that even purely Hamiltonian dynamics with both regular and chaotic phase space structures (75–77), or even with complete chaos (78–80), is capable of generating ratchet effects. As such, there is a renewed interest in considering a number of variants of the KR in an effort to observe and understand ratchet effects. For example, delta-kicked systems with an alternating kicking period and an asymmetric kicking potential (76, 78, 79), or with multiple external fields (77) have been considered.

Although not often thought of as such, the basic idea behind these studies, i.e., to manipulate spatial or temporal symmetry properties to induce a directed current,

is not new from a coherent control perspective. Indeed, more than fifteen years ago Kurizki et al. (81) proposed a simple bichromatic coherent control scenario that can generate photocurrents in semiconductors without a biased voltage. This proposal and its various extensions (82, 83) have been experimentally realized (84–86). Related symmetry-breaking control scenarios designed to manipulate chiral processes are reviewed elsewhere (87).

Here we discuss an entirely different type of Hamiltonian control effect (49) in a model chaotic system called a ratchet accelerator. This system can produce accelerating directed transport in the classical limit without a net external force. The model (49) is based upon large transporting islands in the classical phase space plus a second kicking field that breaks the spatial symmetry. With the same notation as above, the Hamiltonian is given by

$$H^{ratchet}(\hat{L}, \theta, t) = \hat{L}^2/2I + \lambda \cos(\theta) \sum_n f_M(n)\delta(t/T - n) - \lambda' \sin(2\theta) \sum_n \delta(t/T - n), \quad 9.$$

where λ' denotes the strength of a second kicking field with the kicking potential $\sin(2\theta)$, where θ is understood as a variable in an extended phase space, i.e., $\theta \in (-\infty, +\infty)$.

Figure 8*a* shows (for $\kappa = 3.8$, $\lambda'/\lambda = 0.2/3.8$, and $M = 2$) that upon introducing the small-amplitude second kicking field, the classical transporting islands no longer appear in pairs as were seen in Figures 3*b* and 3*d*. Rather, the spatial symmetry of the phase space structures is clearly broken. In particular, all the trajectories on the transporting island seen in Figure 8*a* will increase $\tilde{L}$ by approximately π after each kicking period T. The remaining part of the phase space cell is exclusively occupied by the chaotic sea: there does not exist a similar transporting island that reduces $\tilde{L}$ in a linear fashion.

For a classical ensemble that uniformly covers the entire phase space cell shown in Figure 8*a*, the spatial and temporal periodicity of the system implies that the average acceleration rate is zero (75), i.e.,

$$a_c A_c + \pi A_r = 0, \quad 10.$$

where A_c and A_r denote the areas of the chaotic sea and the transporting regular region, and a_c denotes the average acceleration rate for those trajectories in the chaotic sea. Consider now an initial classical ensemble described by $\tilde{L} = 0$ and $\theta \in (-\infty, +\infty)$. Because this initial ensemble is entirely located in the chaotic sea (note that the structure of the entire phase space is a simple repetition of what is seen in Figure 8*a*), Equation 10 predicts that the average acceleration rate of the classical ensemble is given by $-\pi A_r/A_c$, the negative sign indicating that more trajectories travel to negative θ. That is, even though the average force of the kicking fields is zero and the initial classical ensemble is both spatially symmetric and time-reversal invariant, the magnitude of the classical current, defined as the

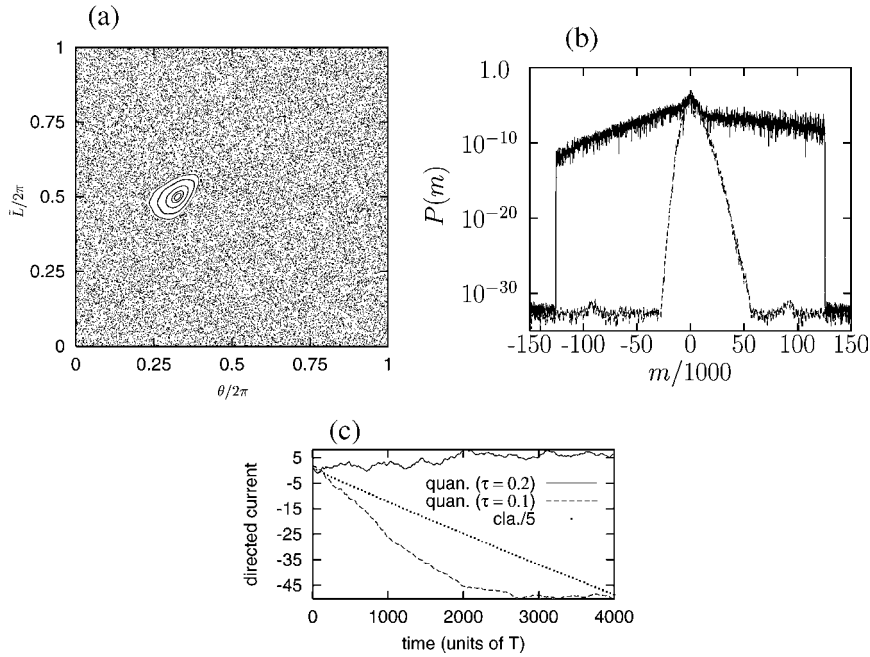

Figure 8 Dynamical behavior of a classical ratchet accelerator and the associated quantum system. (*a*) Classical phase space structure of the ratchet accelerator; (*b*) the probability $P(m)$ of finding the quantum system in the state $|m\rangle$ after 4000 kicks, for two values of the effective Planck constant τ (*solid line* is for $\tau = 0.1$ and *dashed line* is for $\tau = 0.2$); and (*c*) classical directed current (divided by a factor of five) versus the quantum directed current.

ensemble averaged value of $\tilde{L}$, will increase linearly with time. It can also be proved that as time evolves the variance of momentum becomes less and less important as compared with the current (49).

The question is then how this ratchet accelerator manifests itself in the corresponding quantum system if it is far from the classical limit. Figure 8*b* shows the associated distribution function $P(m)$ after 4000 kicks for two values of τ. It is clearly seen that $P(m)$ is asymmetric: the probability of observing a positive m can be much higher than that of observing a negative m. This is due to the stickiness of the boundary between the classical regular structure and the chaotic sea seen in Figure 8*a*, and the fact that the quantum ensemble, initially located in the chaotic sea, can tunnel to the transporting islands. Because the chaotic sea and the transporting islands have opposite acceleration signs (see Equation 10), the quantum tunneling between them (46) necessarily decreases the net current. Figure 8*c* displays a detailed quantum-classical comparison in terms of the directed current. In

the case of $\tau = 0.2$, the quantum net current, defined as $\langle \hat{L}\tau/\hbar \rangle$, is in the opposite direction of the classical current. This is unlike other observations of tunneling-induced current reversal in quantum Brownian motion (88), as the tunneling here is between a chaotic sea and a regular region and this system is totally isolated from the environment. In the case of $\tau = 0.1$, the quantum current does increase almost linearly for as many as 2000 kicks; the average increase rate is about three times smaller than in the classical case. This suggests that $\tau = 0.1$ seems to be small enough to achieve directed quantum current that increases linearly with time without using a biased external field. However, as seen in Figure 8*c*, due to the dynamical localization in quantum delta-kicked systems, the quantum directed current cannot grow all the time. These results indicate that the ratchet accelerator is an ideal system for studying quantum-classical differences in the presence of anomalous diffusion.

It would be of great interest to consider a molecular realization of the ratchet accelerator. As suggested by Equations 4, 6, and 9, diatomics subject to both microwave field and off-resonance laser field, whose polarization directions are perpendicular to one another, are a possible candidate. However, because of the subtle difference between kicked diatomics and the KR (44), detailed calculations using a three-dimensional rigid rotor model of kicked diatomics should be carried out to guide the experimental studies.

3. COHERENT CONTROL OF PHOTODISSOCIATION REACTIONS IN THE CLASSICALLY CHAOTIC REGIME

Coherent control was initially introduced to influence chemical reactions (7, 8). Because chaos can occur in molecular systems (14, 15), it is of interest to examine whether chaos does, or does not, affect the feasibility of quantum control of bond breaking. In a simple scenario for the coherent control of photodissociation reactions, a bichromatic laser field is used to excite a coherent superposition of two bound eigenstates $|E_1\rangle$ and $|E_2\rangle$ on the electronic ground state $|g\rangle$, with energies E_1 and E_2 (7). The wavefunction of the system in the absence of the control field is then given by

$$|\psi(t)\rangle = |g\rangle[c_1|E_1\rangle \exp(-iE_1t/\hbar) + c_2|E_2\rangle \exp(-iE_2t/\hbar)], \qquad 11.$$

where c_1 and c_2 are complex coefficients, and t is the time. The light field can be written as

$$\epsilon(t) = \int d\omega\, \epsilon(\hbar\omega) \cos(\omega t + \phi_\omega), \qquad 12.$$

where $\epsilon(\hbar\omega)$ is the electric field amplitude at frequency ω and ϕ_ω is the associated laser phase. Given the Born-Oppenheimer approximation, the system wavefunction in the presence of the control field can be described by

$$|\Psi(t)\rangle = |g\rangle[c_1|E_1 > \exp(-iE_1t/\hbar) + c_2|E_2\rangle \exp(-iE_2t/\hbar)]$$
$$|e\rangle \left[\sum_{f,q} \int dE\ B(E, f, q|t)|E, f, q^-\rangle \exp(-iEt/\hbar)\right], \quad 13.$$

where $|E, f, q^-\rangle$ is an eigenstate of the system Hamiltonian that correlates with photodissociation fragments in the q arrangement, in the internal state f, at total energy E, and in the electronic state $|e\rangle$.

Denote R as the branching ratio between two arrangement channels q_1 and q_2 at total energy E,

$$R \equiv \frac{\sum_f |B(E, f, q_1|t \to \infty)|^2}{\sum_f |B(E, f, q_2|t \to \infty)|^2}. \quad 14.$$

Then first-order perturbation theory gives

$$R = \frac{\sum_{j=1,2} |c_j|^2 |\bar{\epsilon}(E - E_j)|^2 \mu_{jj}^{q_1} + c_1 c_2^* \bar{\epsilon}(E - E_1)\bar{\epsilon}^*(E - E_2)\mu_{12}^{q_1} + c.c.}{\sum_{j=1,2} |c_j|^2 |\bar{\epsilon}(E - E_j)|^2 \mu_{jj}^{q_2} + c_1 c_2^* \bar{\epsilon}(E - E_1)\bar{\epsilon}^*(E - E_2)\mu_{12}^{q_2} + c.c.}, \quad 15.$$

where

$$\mu_{ij}^q \equiv \sum_f \langle E_i|d_{e,g}|E, f, q^-\rangle\langle E, f, q^-|d_{e,g}|E_j\rangle, \quad 16.$$

$\bar{\epsilon}(\hbar\omega) \equiv \epsilon(\hbar\omega)\exp(-i\phi_\omega)$, and *c.c.* denotes the complex conjugate of the preceding term. Equation 15 clearly shows that by changing the magnitude and phase of the laser field and/or the coefficients c_1 and c_2, the quantum interference terms such as $c_1 c_2^* \bar{\epsilon}(E - E_1)\bar{\epsilon}^*(E - E_2)\mu_{12}^{q_1}$ can be altered, leading to the control of the branching ratio R.

The above control scenario makes no reference to the underlying classical dynamics, suggesting that it should still work even when the initial state is in the classically chaotic regime. This is confirmed by a recent study of the branching photodissociation reaction $CH_2Br + I \leftarrow CH_2BrI \rightarrow CH_2I + Br$ by Abrashkevich et al. (45). They treated CH_2BrI as a pseudo-linear-triatomic molecule, composed of the I, the CH_2 group, and the Br atom, and constructed three empirical potential energy surfaces, whose parameters are determined by fitting the results to all the available experimental data (89), including the A and the B bands absorption spectra and the I/Br branching ratios at 193.3 and 248.5 nm.

Figure 9 displays a computational example of coherent control of the I/Br branching ratio in the CH_2BrI photodissociation reaction. Here $\exp(i\theta_j)f_j \equiv \bar{\epsilon}(E - E_j)c_j$ $(j = 1, 2)$, $S \equiv 1/(1 + |f_1/f_2|^2)$, $2\pi\hbar c/(E - E_1) = 280$ nm, and the initial superposition state comprises two highly excited bound states with energies $E_1 = -0.128018$ au and $E_2 = -0.128008$ au. These two energies are approximately 40 kcal/mol above the ground vibrational state, well above the energy threshold of the onset of classical chaos for the electronic ground state of CH_2BrI (90). As seen from Figure 9, the branching ratio ranges from $R = 0.4$ at

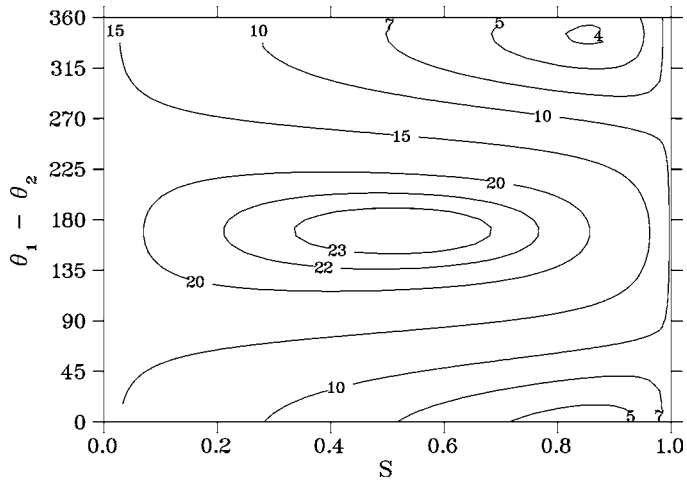

Figure 9 Coherent control of the I/Br branching ratio ($\times 10$) of the CH_2BrI photodissociation in the classically chaotic regime, using a superposition of two highly excited states that are about 15 kcal/mol below the $CH_2Br + I$ dissociation threshold. From Reference (45) with permission.

$S = 0.86$, $\theta_1 - \theta_2 = 345.6^\circ$ to $R = 2.36$ at $S = 0.52$, $\theta_1 - \theta_2 = 172.8^\circ$. This corresponds to a decrease of R by 56.7% relative to the initial state solely given by $|E_1\rangle$ (where $R = 0.93$) and to an increase by 38.9% relative to an initial state solely given by $|E_2\rangle$ (where $R = 1.7$). Extensive control is also observed when superposition states of even higher-lying energy levels (45) are prepared. Clearly then, superpositions of highly-excited states in the classically chaotic regime can also provide the high quality of control expected from superpositions of low-lying states.

The situation is somewhat more complicated if the continuum states $|E, f, q^-\rangle$ are chaotic. Qualitatively, this is the case if the classical dynamics displays a long-lived collision complex at energy E, whose lifetime is longer than the inverse of the Lyapunov exponent. Quantum mechanically, the analog is the existence of a long-lived resonance at energy E. If this resonance is ideal (91), then the Bohr assumption holds (14) and the cross section $\sigma_q(i)$ for the formation of product arrangement q starting in state i satisfies

$$\sigma_q(i) = P(i \to r)\sigma'(r \to q), \qquad 17.$$

where r denotes the intermediate resonance and $P(i \to r)$ denotes the probability of forming r from state i. From Equation 17 the ratio of product states in two product arrangement channels is given by $\sigma_q(i)/\sigma_{q'}(i) = \sigma'(r \to q)/\sigma'(r \to q')$, which is independent of the initial state. Hence, in this case the dynamics cannot be controlled by varying the coherence characteristics of the initial state. Rather,

the only type of coherent control one might envision in this ideal resonance case is attained by altering the character of the intermediate resonance. Note that these conclusions apply only when all products go through the same resonance. When this is not the case, such as in F + HD scattering, control in the presence of resonance can be extensive (91).

4. A PHASE CONTROL APPROACH TO NONADIABATICITY-INDUCED QUANTUM CHAOS

Because coherent control emphasizes quantum interference effects that can be altered at will, it also provides a unique tool for studying atomic and molecular quantum processes. For example, Reference 48 considers a phase control approach to simulating a special type of quantum chaos that can occur in molecular dynamics: quantum chaos induced by the nonadiabatic transitions between different electronic potential surfaces (92–95). Space considerations prevent a description of this approach. Note, however, that it provides a means of adjusting the degree of adiabaticity in a laser-excited three-level system to allow for control of the nonadiabatic dynamics.

5. CONCLUDING REMARKS

The results reviewed above indicate that coherent control can be applied to those quantum systems that have a chaotic classical limit and can be very useful in understanding the quantum dynamics as compared with the underlying classical dynamics. In particular, even extremely simple control schemes, such as those using initial state coherence, periodic field reversal, or multiple kicking fields, may be used to manipulate classically chaotic quantum dynamics. The resultant controlled quantum systems have also revealed a variety of intriguing quantum phenomena that are of importance to the study of quantum chaos and quantum-classical correspondence. These include: (*a*) faster-than-classical quantum anomalous diffusion, (*b*) coherent control that is based upon the quantum tunneling between regular phase space structures and a chaotic sea, (*c*) the manifestations of classical phase space structure in the quantum dynamics with its area much smaller than the effective Planck constant, (*d*) nonexponential lineshape of dynamical localization, (*e*) current reversal induced by quantum coherence effects in a ratchet accelerator, and (*f*) nonadiabaticity-induced quantum chaos simulated in an optical lattice. Similarly, we have noted both the ability to control scattering systems where one channel is dominated by a resonance, and photodissociation from chaotic states.

A more ambitious goal is to consider coherent control in classically chaotic systems with many degrees of freedom, where issues related to the quantum resonance character, noted above, still remain to be resolved. We note, however, that recent studies of intramolecular energy transfer in organic molecules (39, 40) have shown

that energy relaxation in large molecules can occur within a manifold whose dimension is much smaller than that predicted by global ergodicity. If this is the case, then the results described above for low-dimensional classically chaotic systems may be directly relevant to consideration of such high-dimensional systems.

Finally, we note that very recent studies on quantum control in classically chaotic systems (96, 97) further support the view that coherent control can be a powerful tool in manipulating quantum chaos.

ACKNOWLEDGMENTS

This work was partially supported by the U.S. Office of Naval Research and the Natural Sciences and Engineering Research Council of Canada. J.G. thanks Prof. Stuart Rice for his encouragement.

LITERATURE CITED

1. Shapiro M, Brumer P. 2003. *Principles of the Quantum Control of Molecular Processes*, New York: John Wiley
2. Shapiro M, Brumer P. 2003. *Rep. Prog. Phys.* 66:859–942
3. Rice SA, Zhao M. 2000. *Optical Control of Molecular Dynamics*, New York: John Wiley
4. Rice SA. 2001. *Nature* 409:422–26
5. Bergmann K, Theuer H, Shore BW. 1998. *Rev. Mod. Phys.* 70:1003–25
6. Rabitz H, de Vivie-Riedle R, Motzkus M, Kompa K. 2000. *Science* 288:824–28
7. Brumer P, Shapiro M. 1986. *Chem. Phys. Lett.* 126:541–546
8. Tannor DJ, Rice SA. 1985. *J. Chem. Phys.* 83:5013–5018
9. Zhu LC, Suto K, Fiss JA, Wada R, Seideman T, Gordon RJ. 1997. *Phys. Rev. Lett.* 79:4108–11
10. Fiss JA, Zhu LC, Gordon RJ, Seideman T. 1999. *Phys. Rev. Lett.* 82:65–68
11. Fiss JA, Khachatrian A, Truhins K, Zhu LC, Gordon RJ, Seideman T. 2000. *Phys. Rev. Lett.* 85:2096–99
12. Frost W. 1972. *Theory of Unimolecular Reactions*, London: Wiley-Interscience
13. Baer T, Hase WL. 1996. *Unimolecular Reaction Dynamics: Theory and Experiments*, New York: Oxford University Press
14. Brumer P, Shapiro M. 1988. *Adv. Chem. Phys.* 70:365–439
15. Zhao M, Gong J, Rice SA. 2005. *Adv. Chem. Phys.* In press
16. Brumer P. 1981. *Adv. Chem. Phys.* 47:201–238
17. Lichtenberg AJ, Lieberman MA. 1992. *Regular and Chaotic Dynamics*, New York: Springer-Verlag
18. Dumont R, Brumer P. 1986. *J. Phys. Chem.* 90: 3509–3516
19. Rice SA. 2000. *J. Stat. Phys.* 101: 187–212
20. Huang GM, Tarn TJ, Clark JW. 1983. *J. Math. Phys.* 24:2608–18
21. Ramakrishna V, Salapaka MV, Dahleh M, Rabitz H, Peirce A. 1995. *Phys. Rev. A* 51: 960–66
22. Tersigni S, Gaspard P, Rice SA. 1990. *J. Chem. Phys.* 93:1670–80
23. Casati G, Chirikov B. 1995. *Quantum Chaos: Between Order And Disorder*, New York: Cambridge University Press
24. Haake F. 1992. *Quantum Signatures of Chaos*, New York: Springer-Verlag

25. Reichl LE. 1992. *The Transition to Chaos in Conservative Classical Systems: Quantum Manifestations*, New York: Springer-Verlag
26. Wilkie J, Brumer P. 1997. *Phys. Rev. A* 55: 27–42
27. Wilkie J, Brumer P. 1997. *Phys. Rev. A* 55: 43–61
28. Gong J, Brumer P. 2003. *Phys. Rev. A* 68: 062103
29. Rice SA, Kosloff R. 1982. *J. Phys. Chem.* 86:2153–58
30. Pattanayak AK, Brumer P. 1996. *Phys. Rev. Lett.* 77:59–62
31. Pattanayak AK, Brumer P. 1997. *Phys. Rev. E* 56:5174–5177
32. Taylor RD, Brumer P. 1982. *J. Chem. Phys.* 77:854–859
33. Ott E, Grebogi C, Yorke JA. 1990. *Phys. Rev. Lett.* 64:1196–99
34. Lai YC, Ding MZ, Grebogi C. 1993. *Phys. Rev. E* 47:86–92
35. Schwieters CD, Rabitz R. 1991. *Phys. Rev. A* 44:5224–38
36. Botina J, Rabitz R, Rahman N. 1995. *Phys. Rev. A* 51:923–33
37. Ciraolo G et al. 2004. *Phys. Rev. E* 69: 056213
38. Assion A, Baumert T, Bergt M, Brixner T, Kiefer B, Seyfried V, Strehle M, Gerber G. 1998. *Science* 282: 919–22
39. Gruebele M, Bigwood R. 1998. *Int. Rev. Phys. Chem.* 17:91–145
40. Gruebele M. 2003. *Theor. Chem. Acc.* 109: 53–63
41. Batista VS, Brumer P. 2002. *Phys. Rev. Lett.* 89:143201
42. Herek JL, Wohlleben W, Cogdell RJ, Zeidler D, Motzkus M. 2002. *Nature* 417:533–535
43. Gong J, Brumer P. 2001. *Phys. Rev. Lett.* 86:1741–74
44. Gong J, Brumer P. 2001. *J. Chem. Phys.* 115:3590–3597
45. Abrashkevich DG, Shapiro M, Brumer P. 2002. *J. Chem. Phys.* 116:5584–92
46. Gong J, Wörner HJ, Brumer P. 2003. *Phys. Rev. E* 68:026209
47. Gong J, Wörner HJ, Brumer P. 2003. *Phys. Rev. E* 68:056202
48. Gong J, Brumer P. 2002. *Phys. Rev. Lett.* 88:203001
49. Gong J, Brumer P. 2004. *Phys. Rev. E* 70:016202
50. Moore FL, Robinson JC, Bharucha CF, Sundaram B, Raizen MG. 1995. *Phys. Rev. Lett.* 75:4598–601
51. Ammann H, Gray R, Shvarchuck I, Christensen N. 1998. *Phys. Rev. Lett.* 80:4111–14
52. Ringot J, Szriftgiser P, Garreau JC, Delande D. 2000. *Phys. Rev. Lett.* 85:2741–44
53. d'Arcy MB, Godun RM, Oberthaler MK, Cassettari D, Summy GS. 2001. *Phys. Rev. Lett.* 87:074102
54. Averbukh ISh, Arvieu R. 2001. *Phys. Rev. Lett.* 87:163601
55. Machholm M, Henriksen NE. 2001. *Phys. Rev. Lett.* 87:193001
56. Leibscher M, Averbukh ISh, Rabitz H. 2003. *Phys. Rev. Lett.* 90:213001
57. Blümel R, Fishman S, Smilansky U. 1986. *J. Chem. Phys.* 84:2604–14
58. Blümel R, Reinhardt WP. 1997. *Chaos in Atomic Physics*, New York: Cambridge University Press
59. Friedrich B, Herschbach D. 1999. *J. Phys. Chem. A* 103:10280–88
60. Hufnagel L, Ketzmerick R, Otto MF, Schanz H. 2002. *Phys. Rev. Lett.* 89: 154101
61. Sundaram B, Zaslavsky GM. 1999. *Phys. Rev. E* 59:7231–34
62. Iomin A, Fishman S, Zaslavsky GM. 2002. *Phys. Rev. E* 65:036215
63. Roncaglia R, Bonci L, West BJ, Grigolini P. 1995. *Phys. Rev. E* 51:5524–34
64. Fishman S, Grempel DR, Prange RE. 1982. *Phys. Rev. Lett.* 49:509–12
65. Lloyd P. 1969. *J. Phys. C* 2:1717–25
66. Satija II, Sundaram B, Ketoja JA. 1999. *Phys. Rev. E* 60:453–58
67. Shepelyansky DL. 1983. *Physica D* 8:208–22
68. Casati G, Guarner I, Shepelyansky DL. 1989. *Phys. Rev. Lett.* 62:345–48

69. Reimann P. 2002. *Phys. Rep.* 361:57–265
70. Astumian RD, Hänggi P. 2002. *Phys. Today* 55:33–39
71. Jung P, Kissner JG, Hänggi P. 1996. *Phys. Rev. Lett.* 76:3436–39
72. Mateos JL. 2000. *Phys. Rev. Lett.* 84:258–61
73. Porto M, Urbakh M, Klafter J. 2000. *Phys. Rev. Lett.* 85: 491–94
74. Flach S, Yevtushenko O, Zolotaryuk Y. 2000. *Phys. Rev. Lett.* 84:2358–61
75. Schanz H, Otto MF, Ketzmerick R, Dittrich T. 2001. *Phys. Rev. Lett.* 87: 070601
76. Cheon T, Exner P, Seba P. 2003. *J. Phys. Soc. Japan* 72:1087–91
77. Denisov S, Klafter J, Urbakh M. 2002. *Phys. Rev. E* 66:046203
78. Monteiro TS, Dando PA, Hutchings NAC, Isherwood MR. 2002. *Phys. Rev. Lett.* 89: 194102
79. Jonckheere T, Isherwood MR, Monteiro TS. 2003. *Phys. Rev. Lett.* 91:253003
80. Jones PH, Goonasekera M, Saunders-Singer HE, Meacher DR. 2003. preprint quant-ph 0309149
81. Kurizki G, Shapiro M, Brumer P. 1989. *Phys. Rev. B* 39:3435–37
82. Atanasov R, Hache A, Hughes JLP, van Driel HM, Sipe JE. 1996. *Phys. Rev. Lett.* 76:1703–06
83. Bhat RDR, Sipe JE. 2000. *Phys. Rev. Lett.* 85:5432–35
84. Dupont E, Corkum PB, Liu HC, Buchanan M, Wasilewski ZR. 1995. *Phys. Rev. Lett.* 74:3596–99
85. Hache A, Kostoulas Y, Atanasov R, Hughes JLP, Sipe JE, van Driel HM. 1997. *Phys. Rev. Lett.* 78:306–09
86. Stevens MJ, Smirl AL, Bhat RDR, Najmaie A, Sipe JE, van Driel HM. 2003. *Phys. Rev. Lett.* 90:136603
87. Brumer P, Shapiro M. 2004. In *Chiral Photochemistry*, ed. Y. Inone, V. Ramamurthy, pp. 45–106. New York: Marcel Dekker
88. Reimann P, Grifoni M, Hänggi P. 1997. *Phys. Rev. Lett.* 79:10–13
89. Butler LJ, Hintsa EJ, Shane SF, Lee YT. 1987. *J. Chem. Phys.* 86:2051–74
90. Shapiro M, Goelman G. 1984. *Phys. Rev. Lett.* 53:1714–17
91. Zeman V, Shapiro M, Brumer P. 2004. *Phys. Rev. Lett.* 92:133204
92. Heller EJ. 1990. *J. Chem. Phys.* 92:1718–27
93. Blümel R, Esser B. 1994. *Phys. Rev. Lett.* 72:3658–61
94. Schanz H, Esser B. 1997. *Phys. Rev. A* 55:3375–87
95. Fujisaki H, Takatsuka K. 2001. *Phys. Rev. E* 63:066221
96. Takami T, Fujisaki H. 2004. preprint nlin.CD/0402005
97. Takami T, Fujisaki H, Miyadera T. 2004. preprint nlin.CD/0402003

Annual Review of Physical Chemistry
Volume 56, 2005

CONTENTS